Research Square

Preprints are preliminary reports that have not undergone peer review.
They should not be considered conclusive, used to inform clinical practice,
or referenced by the media as validated information.

Study on Moisture Diffusion and Damage Evolution Mechanism of Composite Stiffened Panels in Hygrothermal Environment at Macro-Meso Scales

ZhuoGang Fu
Xi 'an Technological University
LiangMou Hu
Xi 'an Technological University
Yu Feng
fengyu1609@163.com

Air Force Engineering University
Zhe Li
Air Force Engineering University
Yucheng Zhong
Wuhan University of Technology
Shi Yan
Harbin Institute of Technology
Tao An
Air Force Engineering University
Wenjie Cheng
Chinese Academy of Aviation Research (603 Institute)

Research Article

Keywords: Hygrothermal Environment, Mesoscopic Model, Mass Diffusion, Fick's Law

Posted Date: May 4th, 2026

DOI: https://doi.org/10.21203/rs.3.rs-9465806/v1

License: This work is licensed under a Creative Commons Attribution 4.0 International License.
Read Full License

Additional Declarations: No competing interests reported.

Study on Moisture Diffusion and Damage Evolution Mechanism of Composite Stiffened Panels in Hygrothermal Environment at Macro-Meso Scales

ZhuoGang Fu[a], LiangMou Hu[a], Yu Feng[b]*, Zhe Li[b], Yucheng Zhong[c,d], Shi Yan[e], Tao An[b], and Wenjie Cheng[f]

[a]School of Ordnance Science and Technology, Xi 'an Technological University, Xi 'an 710021, China; [b]School of Aeronautical Engineering, Air Force Engineering University, Xi 'an, 710038, China; [c]Hubei Key Laboratory of Theory and Application of Advanced Materials Mechanics, Wuhan University of Technology, Wuhan, 430070, China; [d]Hwaway Technology Corporation Limited, Zhuji, 311800, China; [e]School of Civil Engineering and Architecture, Harbin Institute of Technology, Harbin, 150040, China; [f]Chinese Academy of Aviation Research (603 Institute), Xi 'an 710089, China

Corresponding author. Yu Feng Email: fengyu1609@163.com

Funding information：This work was supported by the National Natural Science Foundation of China under Grant [52472465]; the National Natural Science Foundation of China (Youth Class C) [52505164]; and the National Natural Science Foundation of China (General Program) [52575191].

Study on Moisture Diffusion and Damage Evolution Mechanism of Composite Stiffened Panels in Hygrothermal Environment at Macro-Meso Scales

To reveal the moisture absorption and diffusion mechanism and thermal stress evolution law of composite stiffened panels in hygrothermal environments, a combined experimental and two-scale simulation approach was adopted in this study for systematic investigation. First, a 130-day moisture absorption test was conducted on three carbon fiber/epoxy resin matrix stiffened panel specimens in a water bath environment at 70 °C. The results showed that the saturated moisture absorption content after reaching the engineering dry state ranged from 0.687% to 0.702% (with an average value of 0.695%), and the moisture absorption process exhibited a two-stage characteristic of "rapid increase (0~30 d) - slow saturation (30~120 d)". Second, a macro-meso two-scale simulation model was established: at the macro scale, a three-dimensional model was constructed based on the mass diffusion module to study the overall moisture absorption behavior of the specimens, where the simulated data showed a good fitting degree with the experimental results; at the meso scale, a random fiber distribution model (with a fiber volume fraction of 40%) was developed via Python, the moisture diffusion behavior was equivalently simulated through the heat conduction module, and the thermal stress calculation was implemented by combining the sequential thermal-mechanical coupling method. The results demonstrate that at the macro scale, the moisture absorption rate of thin plate regions is higher than that of thick plate regions, and the entire domain of the specimens basically reaches moisture absorption equilibrium at 130 d. At the meso scale, moisture diffusion induces the formation of micro-damages including micropores, cracks and microdelaminations in the composite panels; fibers exert a significant blocking effect on moisture diffusion, and the random fiber distribution leads to the formation of a wavy diffusion pattern at the diffusion concentration gradient interface, with the diffusion rate in dense fiber regions lower than that in sparse ones. In addition, more pronounced stress concentration occurs in dense fiber regions, and prolonged moisture absorption results in the continuous accumulation of hygroscopic stress. When the stress exceeds the strength threshold of the matrix or fiber/matrix interface (>60 MPa), micropores or cracks initiate at the fiber/matrix interface, which in turn causes the degradation of the mechanical properties of the composites. The research findings of this work provide key experimental data and

a reliable simulation basis for the hygrothermal resistance design of composite structures in the aerospace field.

Keywords: Hygrothermal Environment; Mesoscopic Model; Mass Diffusion; Fick's Law

1. Introduction

Composites, with significant advantages such as high specific strength, high specific stiffness, corrosion resistance, and strong designability, have been increasingly widely used in the aerospace field [1–3]. Especially in the main load-bearing structures such as aircraft fuselage beams and frames, as well as key components including horizontal stabilizers and vertical stabilizers, composite stiffened panel structures have become core components. However, during actual storage, use, and service, these structures are inevitably exposed to complex environments such as hygrothermal conditions, acid-base salt solutions, and ultraviolet radiation for a long time, among which the impact of hygrothermal environment is particularly prominent [4–6].

The diffusion of water molecules in composites is a complex process jointly regulated by temperature, matrix properties, curing process, and fiber orientation [7]. When composite stiffened panels come into contact with a humid environment, moisture penetrates into the material through diffusion. Due to the significant differences in material properties among fibers, resin matrix, and fiber/resin interface layer, moisture intrusion triggers a series of physical and chemical changes: the uneven distribution of moisture inside the material generates moisture-induced stress [8], leading to moisture absorption expansion of the material, which further causes plasticization of the resin matrix, interface aging, and debonding [9–11]; the pressure generated by the vaporization of internal moisture is sufficient to form microvoids or cracks at the fiber/matrix interface [12]. These changes directly result in the degradation of mechanical properties and the

reduction of load-bearing capacity of composite stiffened panels, which not only shortens their service life but also poses a serious threat to the flight safety of aircraft and other equipment.

To reveal the mechanism of hygrothermal effects, scholars at home and abroad have conducted extensive research. Most scholars believe that the moisture diffusion behavior of composites follows Fick's second law [13–15]. In recent years, VanderMeer et al. carried out hygrothermal fatigue tests on co-bonded composite stiffened panels and found that although moisture can delay the propagation of macro-cracks by improving the ductility of the bonding layer, it will increase the risk of fiber-matrix interface debonding [16]; Rocha et al. combined 1D moisture absorption tests and meso-scale observations and found that the fiber-matrix interface diffusion resistance at 70°C decreased by 40% compared with that at room temperature, with a corresponding diffusion coefficient of 3.2×10^{-9} m²/s, clarifying the temperature-sensitive characteristics of the interface state [17]; Mei et al. conducted accelerated moisture absorption tests on carbon fiber composite sandwich panels at three different temperatures (30°C, 55°C, and 80°C) and investigated the effect of hygrothermal aging on their compressive mechanical properties [18]; Feng et al. performed hygrothermal aging tests on composite stiffened panels by immersing them in distilled water at 70°C until moisture saturation [19]; Zhang et al. [20] proposed a two-stage moisture absorption model based on the Fick moisture absorption model and considering the different thicknesses of various parts of the stiffened panel. This model holds that the thinner regions of the stiffened panel first reach moisture absorption equilibrium, followed by the thicker regions until they reach equilibrium. Therefore, theoretically, the composite can be divided into two moisture absorption stages, and the model can well describe the moisture absorption law of composite stiffened panels. Feng Yu et al. [21] studied the mechanical properties of

CCF300/5228A composite stiffened panels in the moisture-saturated state. In this study, first, moisture absorption tests were carried out in a hygrothermal environment of 70°C/95% RH (relative humidity) to make the stiffened panels reach moisture saturation. The buckling half-wave directions of the skin in the cross-section of the two types of specimens were exactly opposite, and the failure location of the moisture-saturated stiffened panels had high uncertainty.

Aiming at the above research gaps, this study conducts a systematic investigation by combining experimental tests and dual-scale simulations: at the macro scale, a three-dimensional model is constructed based on the mass diffusion module to reproduce the overall moisture absorption distribution law of the stiffened panel, and the model accuracy is verified through the 70°C water bath test; at the meso scale, a random fiber distribution model (with a fiber volume fraction of 40%) is generated using Python, and the sequential thermal-stress coupling method is used to explore the influence of fiber spacing and aggregation state on diffusion distribution and stress concentration.

2. Tests on Composite Stiffened Panels

2.1 Test Specimens

Two types of carbon fiber/epoxy resin-based prepregs were used to fabricate the test specimens: one was unidirectional tape UDBA9916-/HF10A-3K with a thickness of 0.125 mm; the other was plain weave fabric BA9916-HFW220TA with a thickness of 0.23 mm. The overall structure of the composite stiffened panel specimens, which includes the typical features of stiffeners and skin, is shown in Fig 1. The planar dimensions of the skin are 200 mm (length) × 150 mm (width), and its specific geometric shape is shown in Fig 2(a); the side profile of the stiffener is "I"-shaped, and its detailed geometric dimensions are shown in Fig 2(b). To ensure the reliability of the test results,

a total of 3 specimens were prepared, numbered 1#, 2#, and 3# in sequence.

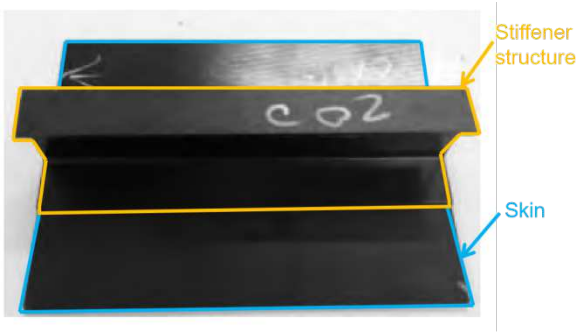


Fig.1 Test specimens

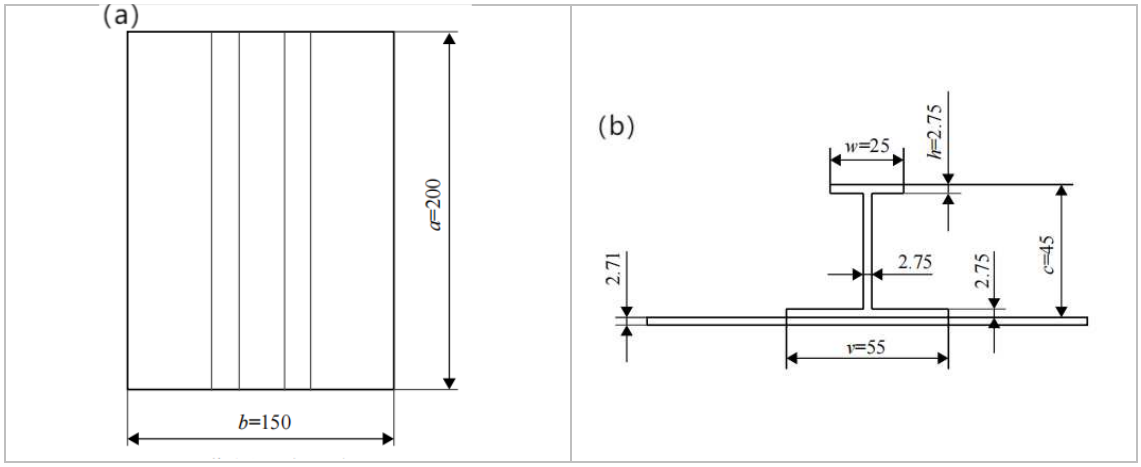


Fig.2 Geometric dimensions of the test specimen (Unit: mm), specific geometric shape of the skin plane (a), geometric dimensions of stiffener side surfaces (b).

2.2 Test Method and Results

Before conducting the moisture absorption test, the specimens were placed in a 70°C drying oven for drying pretreatment. An electronic balance with an accuracy of 0.001 g (as shown in Fig 3) was used to weigh the mass every 24 hours until the mass change of the specimen was less than 0.01% for 3 consecutive measurement cycles. At this point, the specimen was considered to have reached the engineering dry state, and the drying treatment was stopped. According to the ASTM D5229/D5229M-18 standard [22], the hygrothermal environment for the moisture absorption test was set as a 70°C water bath, and the test was carried out in a hygrothermal environmental chamber (with a temperature

control accuracy of ±3°C, as shown in Fig 4). During the moisture absorption process, the mass of the specimen was weighed every 24 hours. According to the standard, the criterion for moisture absorption saturation is that the mass change of the specimen is less than 0.01% for 3 consecutive measurement cycles.

During weighing, the specimen was taken out of the water bath, and its surface moisture was quickly wiped dry with filter paper before immediate weighing. The moisture absorption content M was calculated using Formula (1) (where mi is the mass of the specimen in the i-th cycle, and m0 is the mass of the specimen in the engineering dry state); the moisture absorption content change ΔM between adjacent cycles was determined using Formula (2):

$$M = \frac{m_i - m_0}{m_0} \tag{1}$$

$$\Delta M = \frac{m_i - m_{i-1}}{m_i} \tag{2}$$

Due to differences in the initial mass of each specimen, the mass change laws of the 3 specimens with moisture absorption time were plotted in Fig 5, where the abscissa represents the moisture absorption time and the ordinate represents the specimen mass. The initial masses of specimens 1#, 2#, and 3# were 233.855 g, 233.349 g, and 231.661 g, respectively. After 130 days of moisture absorption, their masses increased by 1.641 g, 1.623 g, and 1.592 g, corresponding to saturated moisture absorption contents of 0.702%, 0.696%, and 0.687%, respectively. To reduce the impact of test errors on the test results, the test data were averaged, and the results are shown in Fig 3.

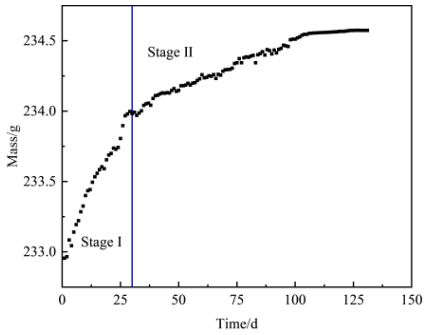


Fig.3 Variation trend of the average results of the 3 specimens

It can be seen from the Fig that in the early stage of the moisture absorption test, the mass of the specimen increased rapidly (this stage lasted approximately 0–30 days). When the moisture absorption time exceeded 30 days, the mass growth rate of the specimen slowed down significantly until it stabilized. After 120 days, the mass of the specimen basically no longer increased, and it can be considered that the specimen had reached the engineering moisture absorption equilibrium state at this time.

3. Moisture Absorption-Diffusion and Sequential Thermal-Mechanical Coupling Simulation Method

3.1 Comparison of Mass Diffusion and Heat Transfer Characteristics

At the meso scale, the mass diffusion behavior is mainly analyzed through the heat transfer module. Compared with the mass diffusion module, the heat transfer module has the advantage that the heat transfer analysis results can be directly used as the initial stress state for static analysis without complex result conversion.

In the mass diffusion module, the moisture absorption-diffusion process is expressed through the node concentration field obtained by the module; in the heat transfer module, the node temperature field is used to equivalently replace the node concentration field, and then in the subsequent thermal stress analysis, the temperature field data are input as predefined field variables into the stress field analysis to calculate

the stress caused by temperature. At this point, the calculated thermal stress is the stress induced by moisture absorption. Therefore, it is first necessary to solve the equivalent relationship between the theories of heat transfer and mass diffusion.

The mass diffusion module can be used to simulate mass diffusion driven by temperature gradient, concentration gradient, or pressure gradient. The governing equation of this module is an extended form of Fick's equation. During the simulation, it is necessary to consider the solubility of the diffusing substance in the matrix material and the mass diffusion driven by temperature gradient or pressure gradient. The basic variable in the simulation (also the degree of freedom of the meshed nodes) is the normalized concentration, which is generally regarded as the driving force for the diffusion of the diffusing substance, and its expression is:

$$\phi = \frac{c}{s} \tag{3}$$

where: c is the concentration of the diffusing substance; s is the solubility of the diffusing substance ($0 \leq s \leq 1$).

The mass diffusion rate is described using Fick's first law under steady-state diffusion, and the expression of Fick's first law under steady-state diffusion is as follows:

$$J = -D\nabla C \tag{4}$$

where: J is the diffusion mass flux density (kg/(s·m²)), and D is the diffusion coefficient (mm²/s).

The expression of Fick's second law is:

$$\frac{\partial C}{\partial t} = -\nabla \mathrm{J} = -\nabla\left(D \times \nabla C\right) \tag{5}$$

where: C is the unit concentration (%); t is the diffusion time (s).

If $\nabla D = 0$, Formulas (4) and (5) can be converted to the following formula:

$$\frac{\partial C}{\partial t} = D\nabla^2 C \tag{6}$$

The heat transfer rate equation is expressed using the Fourier function, and the expression of the Fourier function is as follows:

$$q = -k\nabla T \tag{7}$$

where: k is the thermal conductivity (W/(m·K)), q is the heat flux density (W/m²); T is the temperature (K).

The expression of the thermal diffusion equation is:

$$\frac{\partial T}{\partial t} = -\frac{1}{\rho C_p}\nabla \mathrm{q} = -\frac{1}{\rho C_{\mathrm{p}}}\nabla\left(k \times \nabla T\right) \tag{8}$$

where: C_p is the specific heat capacity (J/(kg·m)); ρ is the density (kg/m³); K is the material thermal conductivity (W/(kg·°C)).

Assuming that the thermal conductivity does not change with time (i.e., $\nabla \mathrm{K} = 0$), Formula (9) is simplified to:

$$\frac{\partial T}{\partial t} = \alpha\nabla^2 T \tag{9}$$

By comparing Formulas (6) and (9), it is found that the two mathematical expressions have exactly the same form. Thus, it can be confirmed that the diffusion laws of temperature and moisture are the same. Therefore, the heat transfer module of ABAQUS can be used for the equivalent simulation calculation of the moisture diffusion

process. At this point, the corresponding relationship between the parameters is shown in Table 1.

Table.1 Analogous Parameters Between Mass Diffusion and Heat Transfer

	Heat Transfer	Mass Diffusion
Variable	T	C
Density	$\rho/(kgcm^{-3})$	1
Conductivity	$k/(W(mK)^{-1})$	$DC_{sat}/(kg(sm))$
Heat Capacity/Moisture Content	$C_p/(J(kgK)^{-1})$	$C_{sat}/(kgm^{-3})$
Expansion Coefficient	$\beta_T/(K\text{-}1)$	β_m

3.2 Moisture Absorption-Diffusion Simulation Model

The model establishment is divided into two categories: one is the macro diffusion model, which uses the mass diffusion module to simulate the diffusion process of moisture concentration distribution, enabling intuitive observation of the moisture absorption process in the three-dimensional state; the other is the meso diffusion model, which uses the heat transfer module to equivalently replace the mass diffusion module, simulates the moisture distribution through the node temperature field, and conducts thermal stress analysis based on this temperature field. Since the macro model has completed the analysis of the overall moisture absorption-diffusion of the stiffened panel, the meso model focuses on exploring the adverse effects of the moisture-induced stress changes of the internal matrix, fibers themselves, and interfaces on the material.

4. Macro Analysis

4.1 Macro Diffusion Model

The macro moisture absorption-diffusion process was simulated using the mass diffusion module: the saturated moisture absorption rate was set to 100%, the temperature was

70°C, and two material parameters (conductivity and solubility) were input; a boundary condition of 0.00702 equilibrium moisture absorption content was applied to all surfaces (including the side surfaces) of the stiffened panel, and the thermal conduction element DC3D20 was used for meshing. The mesh model is shown in Fig 4.

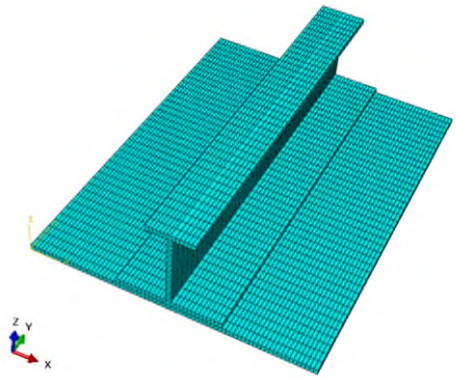


Fig.4 Three-dimensional model of the macro stiffened panel

4.2 Macro Diffusion Model

After the calculation using the mass diffusion module, the CONC variable in the generated post-processing odb file only stores the concentration value corresponding to each node, and the relative moisture increment (i.e., moisture absorption content) cannot be directly obtained from it. Therefore, a Python script was used to extract all node concentration values at each increment step of the model and calculate the weighted average, and finally the curve of the model's moisture absorption content changing with time was obtained. Experimental results are the basis for simulation calculation and the only criterion for verifying the calculation results. The experimental data of moisture increment obtained from the test were compared with the relative moisture increment data obtained from the simulation, and Fig 5 shows the comparison results between the average experimental data and the simulation data.

It can be seen from Fig 5 that the two curves fit well, and the existing errors are normal phenomena:

The test specimen is an orthotropic composite laminate, and its conductivity along the fiber direction (side edge) is lower than that along the thickness direction; however, the simulation adopts a macro perspective and simplifies the moisture absorption-diffusion characteristics to isotropic material properties. Although the error is small and negligible, it is one of the reasons for the higher moisture absorption rate in the early stage of the simulation; during the test, the moisture absorption surface at the bottom of the specimen was in contact with the orifice plate inside the hygrothermal environmental chamber, failing to achieve the complete moisture contact as simulated in the boundary conditions of the simulation, which also led to a smaller moisture absorption content in the early stage of the test.

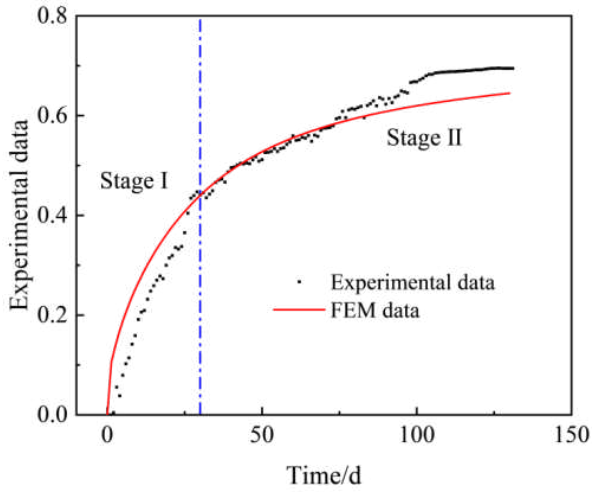


Fig.5 Comparison between average experimental data and simulation data

4.3 Characterization of Macro Moisture Absorption-Diffusion

The transient moisture absorption process of the composite stiffened panel at different times under T=70°C is shown in Fig 6, where the moisture absorption content is expressed as the relative moisture increment ratio. It can be seen from the Fig that with the

continuous change of time, the moisture distribution state in the composite is different: in the early stage of the moisture absorption stage, the surface of the stiffened panel quickly reaches moisture absorption equilibrium; as the moisture absorption time increases, the moisture absorption rate of the thin-panel region is significantly higher than that of the thick-panel region; after 130 days, the entire stiffened panel basically reaches moisture absorption equilibrium.

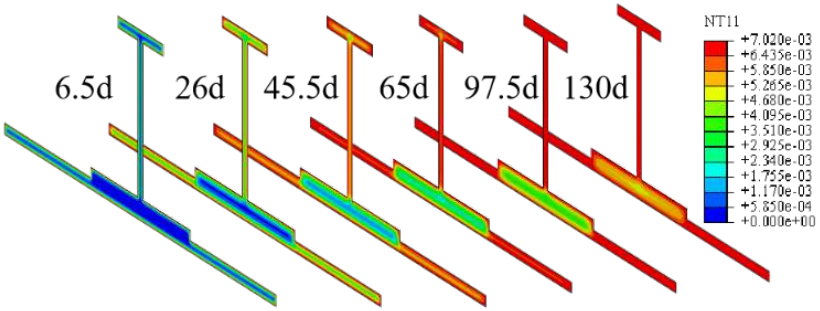
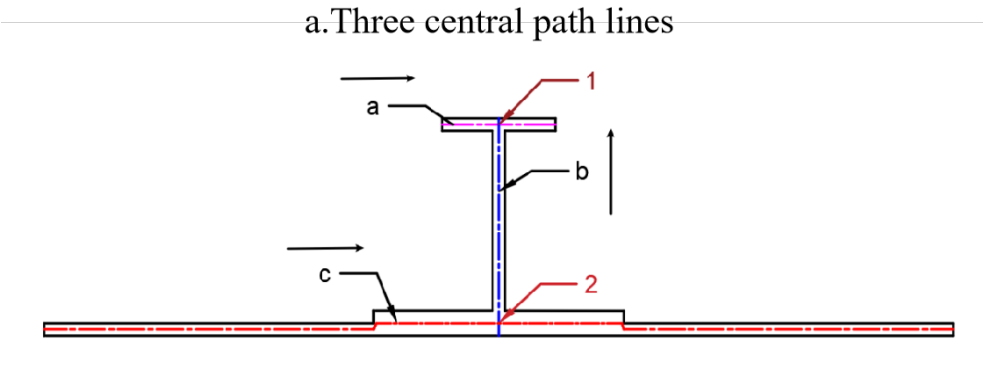


Fig.6 Moisture concentration diffusion process diagram

The moisture absorption-diffusion process of the stiffened panel was further analyzed in detail through the moisture absorption content-displacement diagrams along three central path lines at the cross-section under different moisture absorption times, as shown in Fig 7.



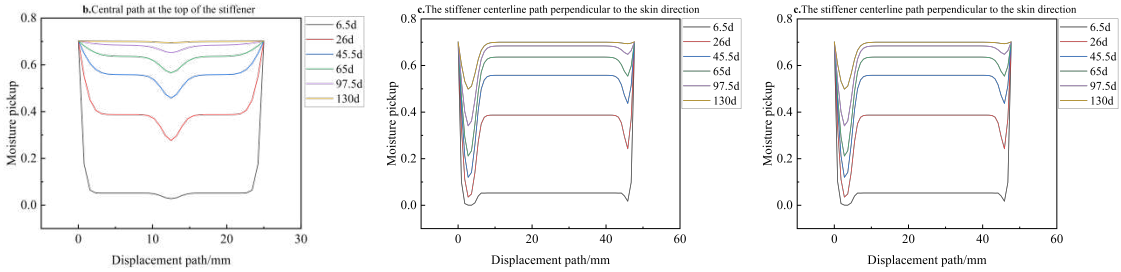


Fig.7 Moisture absorption content-displacement diagrams along three central path lines at the cross-section under different moisture absorption times

The moisture absorption-diffusion characteristics along Path a are as follows: taking a moisture absorption time of 6.5 days as an example, the outer surface of the side edge of the upper panel of the composite stiffened panel first reaches the saturated moisture absorption state. As moisture diffuses inward, when the displacement reaches approximately 0.5 mm, the moisture absorption content decreases significantly. This is because the side edge moisture absorption is considered, and the moisture absorption-diffusion is mainly along the thickness direction. If the equilibrium moisture absorption content in the model boundary condition setting does not consider the side edge moisture absorption, the moisture absorption content along Path a would be a straight line (excluding the moisture absorption boundary at the connection between the vertical panel and the upper stiffener panel); in the range of 0.5 mm–10 mm, the moisture absorption content remains basically stable; when approaching the central region (10 mm–12.5 mm), the moisture absorption content drops to the minimum. With the continuous increase of moisture absorption time, the moisture absorption content at each position along Path a shows an increasing trend until 130 days, when the entire region of the stiffener and upper stiffener panel reaches the equilibrium moisture absorption content.

The multi-time curves of Path b show the restrictive effect of thickness on the diffusion process. It can be seen from the curves that the moisture concentration distribution in the thick-panel part where the bottom of the skin is connected to the lower bottom plate of the stiffened panel is significantly lower than that in other regions. At 130

days, the center point 1 of the upper stiffener panel has reached the equilibrium moisture absorption content, but the area near the center point 2 of the thick-panel part has not yet reached the equilibrium moisture absorption state. This phenomenon directly reflects that the thickness of the composite is a key restrictive factor for moisture absorption-diffusion. Due to the longer mass transfer path of the thick-panel, it takes more time for moisture to complete the overall diffusion.

The curve of Path c (extending from the center point of the left side skin panel to the center point of the thick panel, and then to the center point of the right side skin panel) clearly shows the coupling effect of thickness and diffusion. Under different time periods, the moisture absorption content of the skin panel is higher than that at the center line of the thick panel; in the early stage of moisture absorption (short-time stage), the difference in moisture absorption content between the two parts is small, which is because the overall moisture absorption content is at a low level at this time; with the passage of time, the difference in moisture absorption content between the two first increases and then decreases, and finally all regions tend to the equilibrium moisture absorption content with the extension of time. Combining the analysis of the three paths, it can be concluded that there are significant differences in the moisture absorption rates of regions with different thicknesses, and in the regions where the mass transfer is dominated by the thickness direction, the moisture absorption behavior shows synchronization characteristics.

Observing the entire moisture absorption process from the time dimension through these three path curves, the diffusion rate in the early stage is significantly faster than that in the later stage, which is highly consistent with the "two-stage characteristic" of Fick’s diffusion law. As the moisture absorption time increases, the moisture content inside the material continues to increase, the diffusion rate of moisture inside the composite gradually slows down, and the moisture absorption curve gradually flattens

until it reaches the relative moisture saturation state. The overall process fully conforms to the basic characteristics of Fick's diffusion law.

The internal mechanism of this process can be explained from two aspects: material structure and molecular motion. In the early stage of moisture absorption, defects such as pores and bubbles generated in the pure epoxy resin during the composite preparation process due to process factors become the preferred sites for moisture filling—moisture first occupies the free volume in the form of these pores and bubble defects, and then bonds with the epoxy resin network and causes resin swelling. At this stage, the migration of water molecules is mainly regulated by the concentration gradient inside the epoxy resin, so the moisture absorption-diffusion rate is fast. When moisture absorption enters the "Fick-like plateau stage", a certain amount of moisture has accumulated inside the material: the plasticizing effect of water molecules reduces the glass transition temperature of the polymer material, significantly improving the movement ability of the chain segments in the epoxy resin interpenetrating network, and the probability of long-range mutual movement increases accordingly; under the synergistic effect of swelling stress, the epoxy resin network undergoes structural relaxation, thereby accelerating moisture absorption. At this point, the dominant factor of the moisture absorption process changes from concentration gradient to chain segment movement ability (i.e., structural relaxation). Due to the very slow dynamic process of resin structural relaxation, the moisture absorption rate in the second stage is significantly lower than that in the first stage, and it takes longer for the resin to reach the equilibrium moisture absorption rate. Finally, the moisture shows the characteristic of "gradual diffusion and slow saturation" into the material.

5. Meso Analysis

5.1 Mesoscale Damage Evolution

During the moisture absorption test, the stiffened panels were taken out of the environmental chamber at different time intervals to observe their side surfaces, and the damage evolution process of the stiffened panels during moisture absorption was analyzed. Fig. 8 presents the damage evolution of the stiffened panels during moisture absorption.

It can be observed that prior to moisture absorption (Fig. 8a), the interlaminar bonding was extremely tight without any damages such as cracks or delaminations.

After 15 days of moisture absorption (Fig. 8b), a small number of microvoids were generated in the ±45° plies and 90° ply, which were caused by matrix relaxation within the plies. At 30 days of moisture absorption (Fig. 8c), in addition to a significant increase in microvoids, slight delaminations were observed, including both interlaminar and intralaminar delaminations. When the moisture absorption duration reached 60 days (Fig. 8d), obvious damage propagation occurred: microvoids increased further, slight intralaminar and interlaminar delaminations appeared in most plies, and a small number of cracks were also detected in some non-0° plies.

At 90 and 120 days of moisture absorption (Figs. 8e and 8f, respectively), all types of damages only developed and aggravated slightly compared with the observations at 60 days. Although the specimens underwent an additional 60 days of hygrothermal exposure under the same hygrothermal conditions, the development and aggravation of damages in the latter 70 days were less pronounced than those in the first 60 days. In summary, the damage development of the specimens under the hygrothermal test conditions in this study can be divided into two stages: a rapid damage development stage in the first 60 days and a stage with a significant slowdown in damage development in the latter 70 days.

It is evident that the damage variation law is consistent with the two-stage moisture absorption and diffusion behavior reflected by the moisture absorption content curves from both experiments and simulations. Meanwhile, the curve of moisture absorption weight versus time shown in Fig. 3 can also be divided into two stages: a rapid moisture absorption stage in the early period and a stage with a gradually decelerating moisture absorption rate in the later period.

Fig. 9 shows the schematic diagrams of damage evolution associated with moisture absorption and diffusion, where Fig. 9a is the 3D schematic diagram of the fiber-matrix side surfaces with different ply orientations. This 3D schematic diagram provides an intuitive understanding of the damage modes observed in the same direction for different plies. Fig. 9b is the schematic diagram of damage evolution on the side surfaces of the stiffened panels with different ply orientations, illustrating that the damage modes of the composite panels gradually increased during moisture absorption, and the damage degree increased progressively until it tended to be stable.

Based on the above observations, the following inferences can be drawn: (a) The rapid moisture absorption stage in the early period is not only induced by inherent cracks and porosities; the microvoids, cracks, microdelaminations and other damages generated in the early moisture absorption period can further accelerate the moisture absorption rate in this stage. In contrast, the rate of new microvoids, cracks and microdelaminations generated in the later period is relatively slow, which further exacerbates the difference in moisture absorption rates between the early and late stages. (b) The gradual diffusion of moisture causes matrix swelling, and the resulting fiber extrusion leads to fiber debonding, which in turn generates microdelaminations, matrix microvoids and cracks.

The mesoscale dynamic evolution mechanism and the interactions between fibers and the matrix will be further analyzed via mesoscale model simulations in the subsequent section.

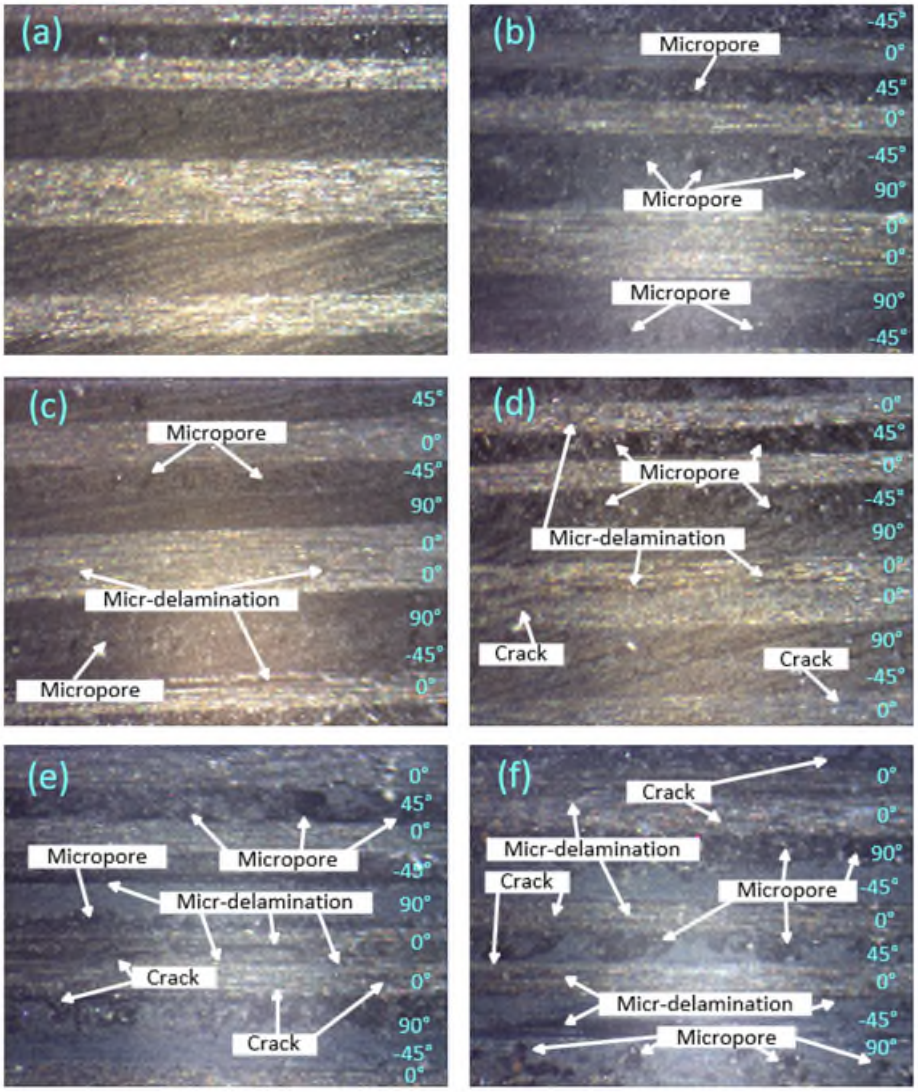


Fig.8 Damage evolution of stiffened panels during moisture absorption, prior to moisture absorption (a), moisture absorption for 15 days (b), moisture absorption for 30 days (c), moisture absorption for 60 days (d), moisture absorption for 90 days (e), moisture absorption for 130 days (f).

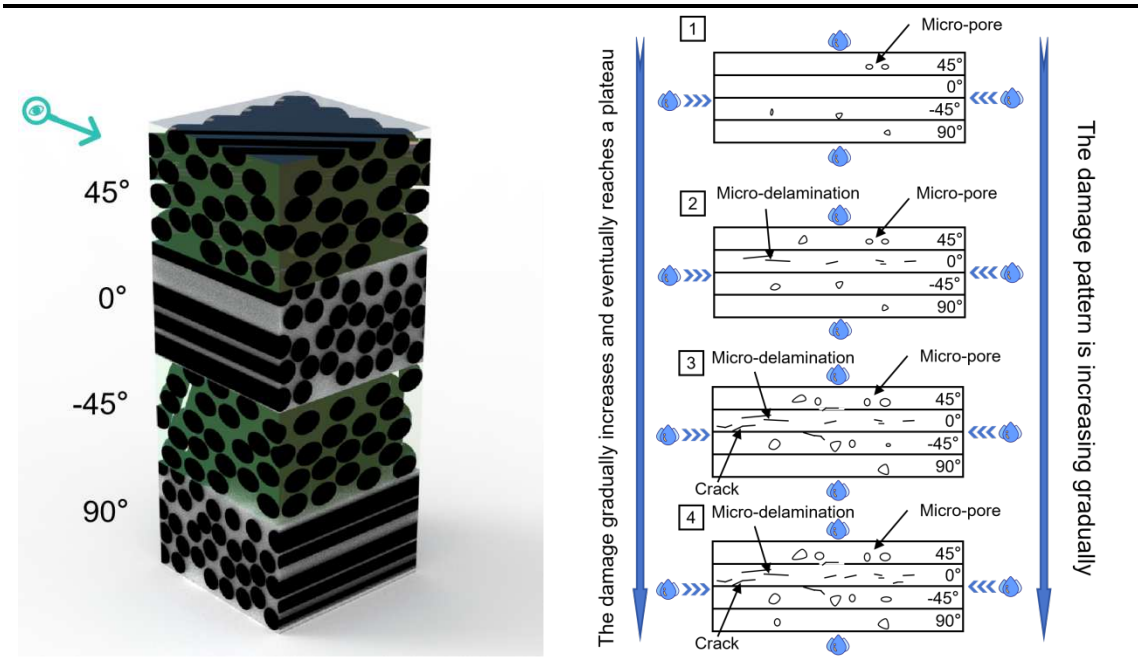


Fig.9 Schematic diagram of damage evolution of stiffened panels during moisture absorption, 3D schematic diagram of fiber-matrix side surfaces with different ply orientations (a), Schematic diagram of damage evolution on the side surfaces of stiffened panels with different plies (b).

5.2 Meso Diffusion Model

Since fibers need to be embedded in the mesoscale diffusion model, a two-dimensional (2D) planar model was established to reduce computational costs and facilitate convergence. The model was designed as a rectangular plane with dimensions of 0.125 × 1.25 mm, and a single ply of the composite stiffened panel was selected for mesoscale investigation.

A random fiber distribution model was developed using Python programming language. During the modeling process, interference judgment was performed on fiber distribution, and a simplified assumption of "non-overlapping fibers" was adopted. Considering that the macroscopic model had already conducted a detailed analysis of diffusion behavior, the actual number of fibers was not strictly matched in this mesoscale model. The core objective of modeling was to investigate the evolution law of

hygroscopic stress within the fibers, matrix, and their interfaces in the stiffened panel during moisture absorption and diffusion by introducing fibers. Fibers were embedded at a fiber volume fraction of 40%, with a total number of 4955 fibers inserted.

The moisture absorption and diffusion module was simulated via the heat conduction module, with the thermal conduction parameters set as listed in Table 2. Mesh generation was performed using the mapped meshing method, which enabled the generation of regular quadrilateral meshes for the complex 2D solid model. The mesh seed size was set to 0.005 mm, and the mesh element type was DC2D8 (8-node 2D thermal conduction element).

The core research objective of the mesoscale model was to focus on the local regulatory mechanism of fiber-matrix interfaces and fiber distribution on moisture diffusion inside the composite, rather than reproducing the multi-surface moisture absorption behavior of the macroscopic global domain. To establish a clear diffusion gradient for accurately capturing the moisture diffusion path and avoid the blurring of phenomena caused by the superposition of multi-directional diffusion, only the left side of the model was designated as the moisture contact surface. Accordingly, the boundary conditions were set as follows: the left surface was assigned the saturated moisture absorption content, while the top, bottom, and right surfaces were set as symmetric boundary conditions. At the initial stage of moisture absorption, the composite was in a dry state (i.e., zero moisture absorption content), and the predefined temperature field was set to 0 to represent the state of no moisture absorption. The mesh model and boundary settings are shown in Fig 10.

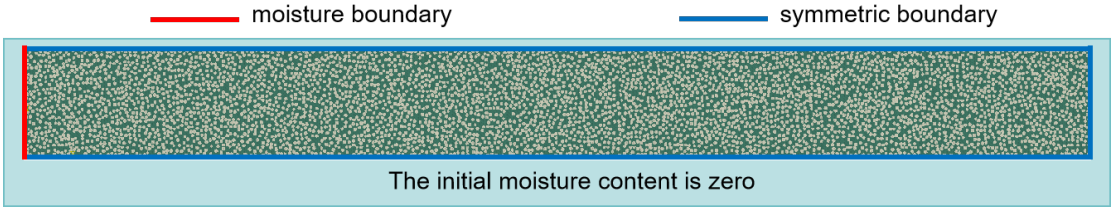


Fig.10 Meso model and boundary condition settings

The thermal stress analysis step is a static analysis step. The parameter settings for thermal stress analysis are shown in Table 3, and the mesh element type is CPE8R. The node temperature field obtained from the heat transfer analysis was set as the predefined field for thermal stress analysis, and the other model parameter settings were consistent with those of the heat transfer analysis.

Table.2 Assignment of Material Properties for Heat Transfer Analysis

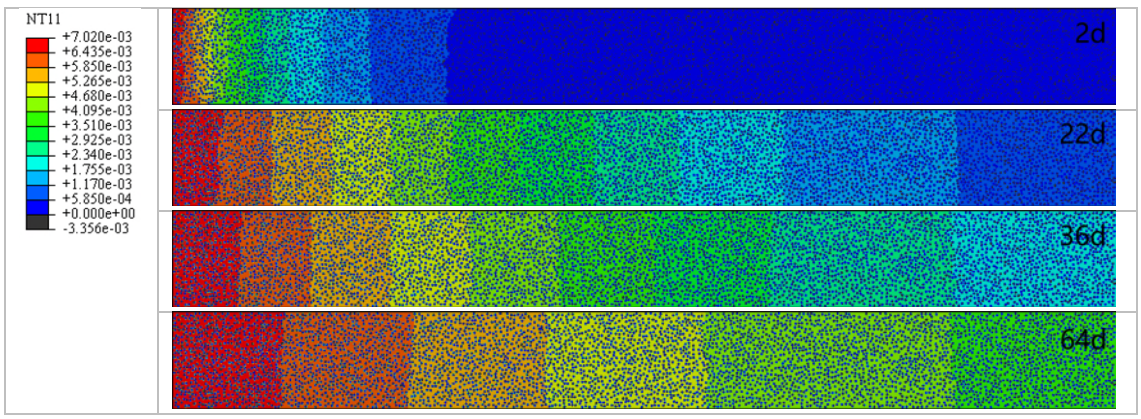
Property	Matrix	CF
$C_p/(J(kgK)^{-1})$	1	1
ρ(kg/m^3)	1	1
$k/(W(mK)^{-1})$	0.02052	0

Table.3 Assignment of Material Properties for Thermal Stress Analysis

Property	Matrix	CF
$C_p/(J(kgK)^{-1})$	1	0
ρ(kg/m^3)	1	0
$k/(W(mK)^{-1})$	0.02052	0
$E(GPa)$	3.45	230
βm	0.324	0
υ	0.35	0.26

5.3 Meso Moisture Absorption-Diffusion and Stress Field Distribution Law

5.3.1 Moisture Absorption-Diffusion Distribution



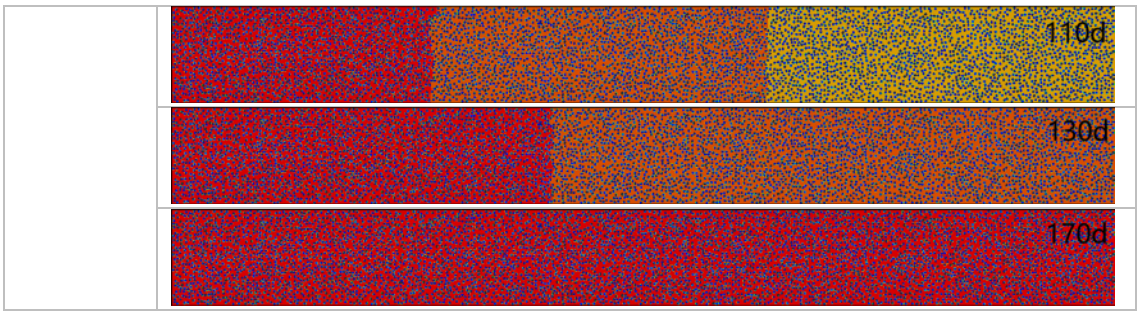


Fig.11 Moisture diffusion diagrams at different moisture absorption times

From the moisture diffusion contours of the mesoscale model in Fig 11, it can be clearly observed that the left surface rapidly reaches saturated moisture absorption immediately upon moisture contact. With the increase in moisture absorption time, the entire model eventually achieves a saturated state, yet the fibers remain in a non-absorptive state at 170 days.

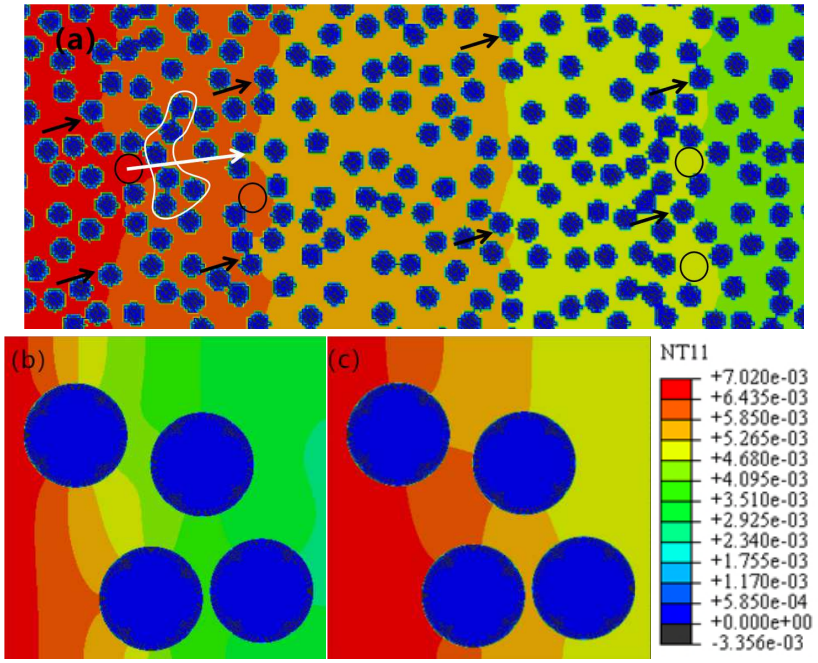


Fig.12 Magnified diagrams of moisture diffusion at different concentration gradients

It can be seen from Fig 11 (moisture diffusion contour at 2 days) that the moisture spreads rapidly in the transverse direction immediately after the left moisture absorption surface comes into contact with moisture. However, the diffusion concentration gradient is not a regular planar interface as observed in the macroscopic model, but exhibits a

wavy undulation that is highly correlated with fiber positions — when the diffusion path approaches the fibers, the moisture flows around the fiber surfaces, forming local diffusion lag zones (clearly indicated by the black arrows in Fig 12a). It can be clearly observed from Figs 10b and 10c (0.1 and 0.2 days) that no moisture absorption occurs in the matrix itself; the fibers block the moisture diffusion paths, leading to the formation of diffusion bypass channels around the fibers, and the diffusion front is ultimately dynamically adjusted with fiber positions. As shown in Fig 10a, the fiber distribution is relatively dense in the area enclosed by the white frame, which exerts a local blocking effect on moisture diffusion paths. Moisture diffusion thus has to penetrate the narrow inter-fiber channels sequentially to proceed further — the moisture absorption content at the starting points of the white arrows is higher than that in the adjacent areas, while it becomes lower than the adjacent areas at the arrow end points after passing through the white-framed area. This indicates that fiber spacing is a key regulatory factor for the moisture absorption rate at the mesoscale: the smaller the spacing, the more tortuous the mass transfer path, and the more significant the diffusion lag effect.

5.3.2 Moisture-Induced Thermal Stress Analysis



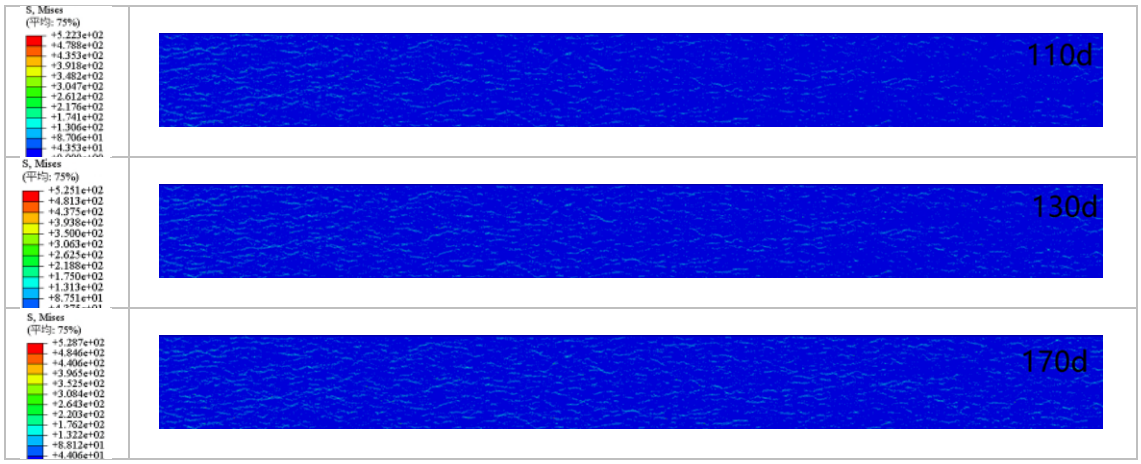


Fig.13 Thermal stress distribution diagrams at different moisture absorption times

It can be observed from Fig 13 that hygroscopic stress propagates along the direction of moisture diffusion with increasing moisture absorption time, and the stress magnitude increases correspondingly. The generation of hygroscopic stress is attributed to the hygroscopic swelling-induced mismatch between the non-absorptive fibers and the moisture-absorptive resin matrix. At the early stage of moisture absorption, this swelling-induced mismatch is insignificant, resulting in a low level of hygroscopic stress.

The entire model was equally divided into five regions along its long side, and the average stress values of different regions and the whole model were extracted at each increment step, as shown in Fig 14 (the regions were divided along the moisture diffusion direction). It can be seen from the overall hygroscopic stress curve and the regional stress curves in Fig 14 that hygroscopic stress can also be roughly divided into two stages: a rapid growth with an approximately linear trend in the early stage, followed by a gradual decrease in the growth rate in the later stage. This two-stage characteristic weakens progressively from Region 1 to Region 5. This is because Region 1, the initial diffusion region, reaches moisture absorption saturation rapidly, leading to the most severe matrix-fiber mismatch; for the subsequent regions, the varying degrees of moisture absorption saturation caused by the sequential moisture diffusion result in different levels of mismatch severity.

Hygroscopic stress values vary among different regions at the same moisture absorption time, yet the stress difference between each region diminishes gradually with increasing moisture absorption time. The decelerated stress growth in the later stage is due to the approaching of moisture absorption diffusion to saturation, which leads to a reduction in hygroscopic swelling of the matrix and a consequent decrease in the rate of stress variation.

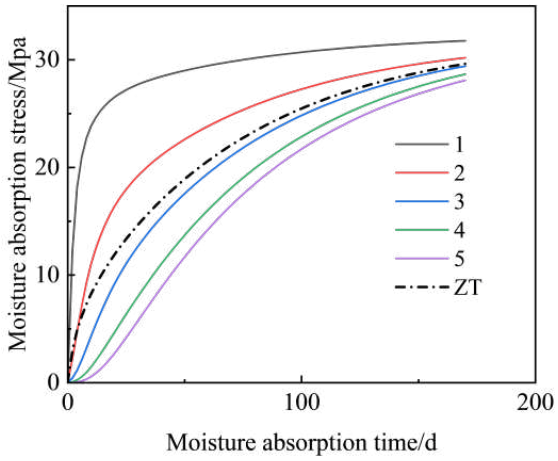


Fig.14 Stress average values of different regions and the whole specimen under different conditions

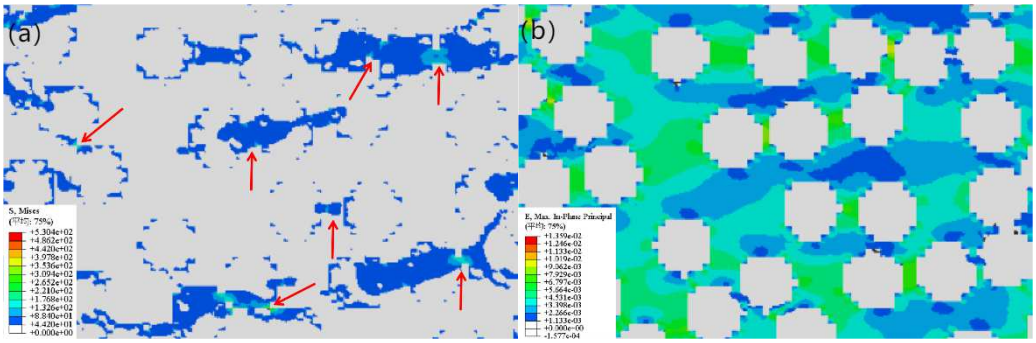


Fig.15 Magnified diagrams of stress and strain, Magnified diagrams of stress (a), Magnified diagrams of strain (b).

It can be seen from Fig 15 that the regions with the fastest hygroscopic stress growth rate occur around fibers and along the fiber-matrix interfaces. The stress growth rate in these regions is not only much higher than that in the bulk matrix, but the stress magnitude is also significantly greater than in other regions. This is visually manifested

in the hygroscopic stress contours as the stress at the fiber-matrix interfaces reaching an extremely high level. The areas immediately surrounding the fibers exhibit relatively low hygroscopic stress due to hygroscopic swelling, while regions with smaller inter-fiber spacing generate significantly higher stress. The magnified strain contours can more intuitively reveal that the random fiber distribution leads to an inhomogeneous distribution of hygroscopic stress within the composite: the closer to the fibers, the higher the hygroscopic strain values, and the regions with the densest fiber packing are where the maximum hygroscopic strain occurs.

To further elucidate the effect of inter-fiber spacing on hygroscopic stress, two fiber distribution models with regular fiber arrangement were established, as shown in Fig 16. For the two models, the center-to-center distance between adjacent fibers was set to 0.1 mm and 0.085 mm, respectively.

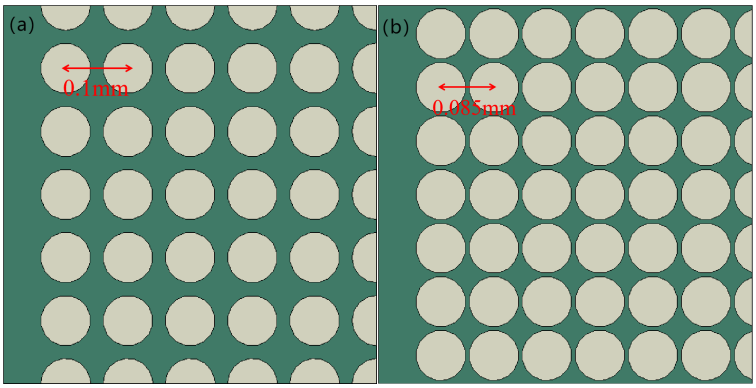


Fig.16 Regular distribution diagrams of two fiber spacings, fiber center-to-center distance: 0.1 mm (a), fiber center-to-center distance: 0.085 mm (b).

Fig 17 presents the hygroscopic stress contours for the two fiber spacing conFigurations. It can be seen from the contours that the maximum equivalent stress for the fiber spacings of 0.1 mm and 0.085 mm is found to be 57.70 MPa and 62.84 MPa, respectively. The maximum stress occurs at the midpoint between adjacent fibers along the moisture diffusion direction. This indicates that inter-fiber spacing is a key factor governing the distribution of hygroscopic stress, with smaller spacing giving rise to

higher hygroscopic stress. For epoxy resin, its tensile strength is typically in the range of 60–100 MPa, thus rendering the resulting stress level considerably high. Prolonged exposure of the composite to such high stress levels, or the occurrence of moisture absorption-desorption cycles during actual service, may lead to severe degradation of its mechanical properties.

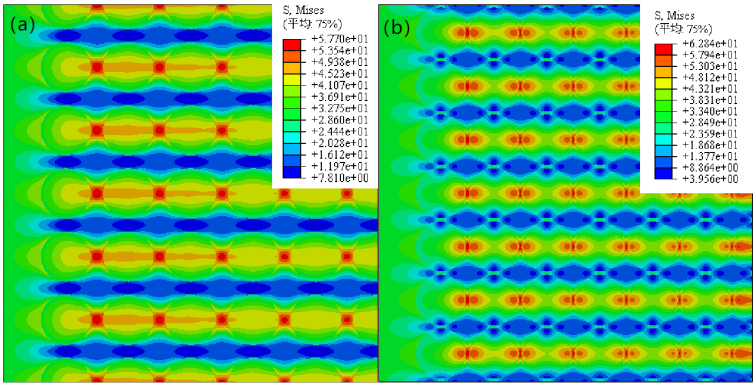


Fig.17 Moisture-induced stress cloud diagrams of two fiber spacing distributions, fiber center-to-center distance: 0.1 mm (a), fiber center-to-center distance: 0.085 mm (b).

Fig 18 shows the hygroscopic stress curves along the fiber boundary for the two fiber spacings at different increment steps, with the path direction indicated at the lower right of the Fig—starting from the center of the left semicircular boundary of the fiber and encircling the fiber for a full cycle. To accurately locate the key stress characteristic regions, three points (A, B, C) are defined on the fiber boundary corresponding to the curves: Point A is the peak stress position on the water-facing side of the fiber (along the moisture diffusion direction), corresponding to the strong fiber-matrix constraint region at the moisture diffusion front; Point B is the valley stress position at the upper and lower ends of the fiber; Point C is the secondary peak stress position on the water-backing side of the fiber (the downstream side of the moisture diffusion direction), corresponding to the weak fiber-matrix constraint region with moisture diffusion lag. The clockwise arc boundaries between the three points are denoted as lAB and lBC, respectively.

For both the 0.1 mm and 0.085 mm fiber spacings, the stress curves exhibit a symmetric two-peak two-valley distribution around the fiber circumference: along the lAB-lBC arc, the stress decreases gradually from the peak at Point A to the valley at Point B, then rises slowly to the secondary peak at Point C.

It can be clearly observed from Fig 18 that at the early stage of moisture absorption, taking increment step 10 of the 0.1 mm spacing as an example (34.12 MPa at Point A, 15.66 MPa at Point B, and 26.50 MPa at Point C), the hygroscopic stress at Point C is lower than that at Point A at the same time. With the increase in moisture absorption time, the stress difference between Point A and Point C gradually approaches zero at the moisture absorption saturation stage (increment step 60: 45.92 MPa at Point A and 45.28 MPa at Point C). This is because Point A directly bears the matrix swelling extrusion stress induced by moisture diffusion: the matrix undergoes preferential hygroscopic swelling and generates intense extrusion stress under the rigid constraint of fibers, with the stress gradient increasing continuously as moisture penetrates the composite. In contrast, Point C is subject to diffusion lag on the water-backing side, leading to a lower degree of matrix swelling compared with the water-facing side; as moisture absorption proceeds to saturation, the matrix swelling degree at Point C becomes consistent with that at Point A. As the stress relief zone at the upper and lower ends of the fiber, Point B has a relatively sufficient space for matrix swelling, resulting in the minimum stress at this position.

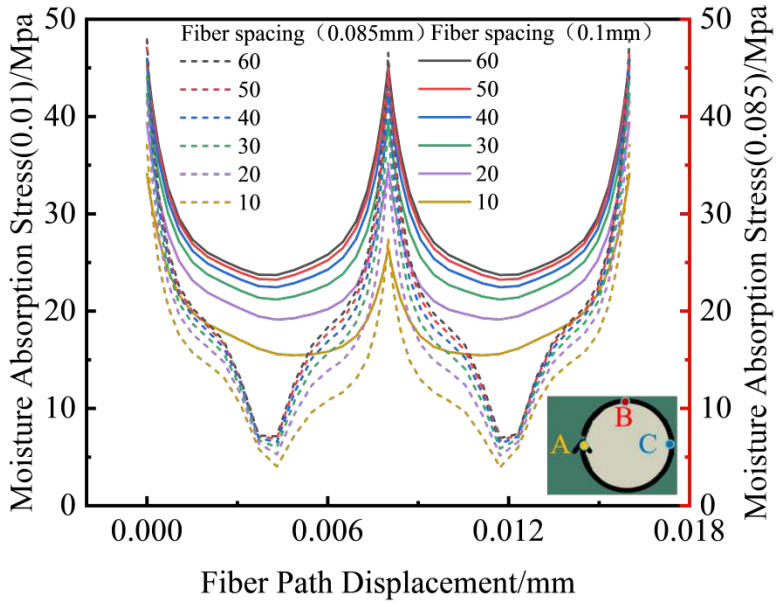


Fig.18 Moisture-induced stress curves along the fiber boundary for two fiber spacings at different increment steps

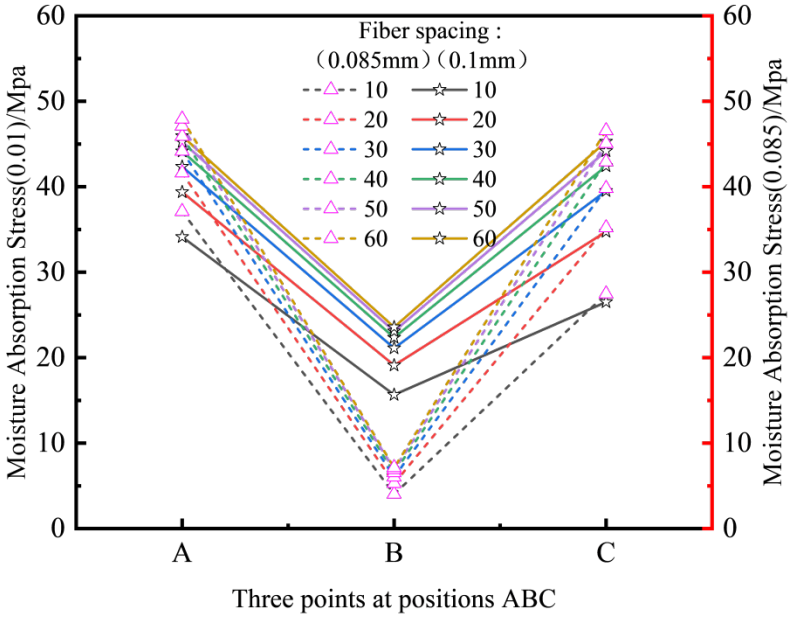


Fig.19 Moisture-induced stress curves at points A, B, and C for two fiber spacings at different increment steps

A comparison of the stress distribution characteristics between the 0.1 mm and 0.085 mm fiber spacings reveals that at the same increment step (moisture absorption time), the Mises stress at the main peak Point A (water-facing side) and the secondary peak Point C (water-backing side) for the 0.085 mm spacing with denser fibers is

significantly higher than that for the 0.1 mm spacing, while the Mises stress at the valley Point B (upper and lower fiber ends) is consistently lower for the 0.085 mm spacing. As illustrated in Fig 19 (taking increment step 10 as an example): for the 0.1 mm spacing, the Mises stress values are 34.12 MPa at Point A, 15.66 MPa at Point B and 26.50 MPa at Point C; for the 0.085 mm spacing, the values are 37.10 MPa at Point A, 4.03 MPa at Point B and 27.46 MPa at Point C.

For the 0.085 mm spacing, the denser fiber arrangement leads to a significant increase in the fiber-matrix contact area compared with the 0.1 mm spacing, subjecting the moisture diffusion-induced matrix swelling to enhanced rigid constraints — at the water-facing Point A, the instantaneous superposition of the extrusion effect from hygroscopic matrix swelling occurs due to preferential moisture contact, and the dense fiber arrangement leaves no buffer space for the constraints, making the stress concentration effect highly prominent. Although the water-backing Point C is affected by diffusion lag, the dense fibers shorten the effective path for transverse moisture penetration, resulting in a faster moisture accumulation rate than that of the 0.1 mm spacing. Consequently, the hygroscopic swelling mismatch between the matrix and fibers intensifies rapidly over time, ultimately leading to higher Mises stress at both Points A and C for the 0.085 mm spacing than the 0.1 mm spacing. The lower Mises stress at Point B for the 0.085 mm spacing is essentially attributed to reduced hygroscopic stress in the upper and lower fiber end regions, which is caused by hindered moisture penetration and restricted matrix swelling induced by the dense fiber arrangement.

6. Conclusions

(1). Under the 70°C water bath environment, the moisture absorption process of the carbon fiber/epoxy resin-based stiffened panel conforms to the "two-stage" evolution

characteristic of Fick's diffusion law: 0–30 days is the rapid moisture absorption stage, 30–120 days is the slow saturation stage, and the engineering moisture absorption equilibrium is reached after 130 days, with the saturated moisture absorption content stably ranging from 0.687% to 0.702%.

(2). The three-dimensional macro model based on the mass diffusion module accurately reproduces the moisture absorption distribution law of the stiffened panel: in the early stage of moisture absorption (<26 days), the surface first reaches saturation, and then moisture penetrates inward along the thickness direction; thickness is the core regulatory factor for overall diffusion, and the thin-panel region has a higher moisture absorption rate than the thick-panel region due to the shorter mass transfer path. The model fits well with the experimental data.

(3). Moisture diffusion induces three types of damage in composite laminates, namely microvoids, cracks and microdelaminations. The mesoscale model reveals the effect of fiber distribution on moisture diffusion and hygroscopic stress: Fibers exhibit a significant blocking effect on moisture diffusion, and the concentration gradient at the diffusion interface presents a wavy undulation that is highly dependent on fiber positions; the smaller the inter-fiber spacing, the more tortuous the mass transfer path and the more significant the diffusion lag effect. The evolution of hygroscopic stress is deeply coupled with the moisture diffusion process, and stress concentration occurs at the fiber-matrix interface due to hygroscopic swelling mismatch, with the stress concentration becoming more pronounced as the inter-fiber spacing decreases — the peak Mises stress of the model with a 0.085 mm spacing reaches 62.84 MPa, which is significantly higher than the 57.70 MPa recorded for the 0.1 mm spacing model. When prolonged moisture absorption causes the hygroscopic stress to exceed the strength threshold of the matrix or fiber-matrix interface (> 60 MPa), microvoids initiate at the fiber-matrix interface and

gradually propagate into cracks; this impairs the internal load transfer path and ultimately leads to the degradation of the composite's mechanical properties.

Author contributions:Z.G.F. mainly conducted moisture absorption tests and moisture absorption simulations, and took charge of manuscript writing. L.M.H. and Y.F. assisted in test preparation. Y.F. also took charge of project administration and funding acquisition, and participated in manuscript review and editing. Y.C.Z., and Z.L. completed macro-meso dual-scale simulations, data analysis, and formal analysis. S.Y., T.A and W.J.C. participated in data curation and editing. All authors reviewed and approved the final manuscript.

Conflict of interest: No potential conflict of interest was reported by the author(s).

Statements and Declarations: The datasets generated during and/or analyzed during the current study are available from the corresponding author on reasonable request.

References

[1] Gogoi R, Maurya A K, Manik G. A review on recent development in carbon fiber reinforced polyolefin composites. Composites Part C: Open Access, 2022, 8: 100279. doi: 10.1016/j.jcomc.2022.100279

[2] Liu S, Ding Y, Feng Y, et al. Low-velocity impact size effect of carbon fiber composite laminates: Experimental and mechanism research. Thin-Walled Structures, 2025;34(6):1153-1173. doi: 10.1080/09243046.2025.2464960

[3] He Y, Tian G Y, Pan M, et al. Non-destructive testing of low-energy impact in CFRP laminates and interior defects in honeycomb sandwich using scanning pulsed eddy current. Composites Part B: Engineering, 2014; 59: 196-203. doi: 10.1016/j.compositesb.2013.12.005

[4] Nandagopal R A, Boay C G, Narasimalu S. An empirical model to predict the strength degradation of the hygrothermal aged CFRP material. Composite Structures, 2020; 236: 111876. doi: 10.1016/j.compstruct.2020.111876

[5] Pivdiablyk I, Rozycki P, Jacquemin F, et al. Experimental analysis of mechanical performance of glass fibre reinforced polyamide 6 under varying environmental conditions. Composite Structures, 2020; 245: 112338. doi: 10.1016/j.compstruct.2020.112338

[6] Zhong Y, Cheng M, Zhang X, et al. Hygrothermal durability of glass and carbon fiber reinforced composites–A comparative study. Composite Structures, 2019; 211: 134-143. doi: 10.1016/j.compstruct.2018.12.034

[7] Behera A, Vishwakarma A, Thawre M M, et al. Effect of hygrothermal aging on static behavior of quasi-isotropic CFRP composite laminate. Composites Communications, 2020; 17: 51-55. doi: 10.1016/j.coco.2019.11.009

[8] Thomason J L, Yang L. Temperature dependence of the interfacial shear strength in glass–fibre epoxy composites. Composites science and technology, 2014; 96: 7-12. doi: 10.1016/j.compscitech.2014.03.009

[9] Johnson, W. S., Mangalgiri, P. D.: Influence of the resin on interlaminar mixed-mode fracture. NASA-TM-87571, 1985.

[10] Cauich-Cupul J I, Pérez-Pacheco E, Valadez-González A, et al. Effect of moisture absorption on the micromechanical behavior of carbon fiber/epoxy matrix composites. Journal of Materials Science, 2011; 46(20): 6664-6672. doi: 10.1007/s10853-011-5619-0

[11] Lu M M, Fuentes C A, Van Vuure A W. Moisture sorption and swelling of flax fibre and flax fibre composites. Composites Part B: Engineering, 2022; 231: 109538. doi: 10.1016/j.compositesb.2021.109538

[12] Ye J Y, Zhang L W. Damage evolution of polymer-matrix multiphase composites under coupled moisture effects. Computer Methods in Applied Mechanics and Engineering, 2022; 388: 114213. doi: 10.1016/j.cma.2021.114213

[13] Zafar A, Bertocco F, Schjødt-Thomsen J, et al. Investigation of the long term effects of moisture on carbon fibre and epoxy matrix composites. Composites Science and Technology, 2012; 72(6): 656-666. doi: 10.1016/j.compscitech.2012.01.010

[14] Mansouri L, Djebbar A, Khatir S, et al. Effect of hygrothermal aging in distilled and saline water on the mechanical behaviour of mixed short fibre/woven composites. Composite Structures, 2019; 207: 816-825. doi: 10.1016/j.compstruct.2018.09.067

[15] Nandagopal R A, Narasimalu S, Chai G B. Study of statistically significant strength degradation of hygrothermal aged CFRP and its weibull analysis. Composites Communications, 2021; 23: 100566. doi: 10.1016/j.coco.2020.100566

[16] van den Akker B P H, Donadon M V, Loendersloot R, et al. The influence of hygrothermal aging on the fatigue behavior and residual strength of post-buckled co-bonded stiffened panels subjected to compressive loading. Composites Part B: Engineering, 2020; 194: 108023. doi: 10.1016/j.compositesb.2020.108023

[17] Rocha I, Van der Meer F P, Nijssen R P L, et al. A multiscale and multiphysics numerical framework for modelling of hygrothermal ageing in laminated composites. International Journal for Numerical Methods in Engineering, 2017; 112(4): 360-379. doi: 10.1002/nme.5542

[18] Mei J, Tan P J, Liu J, et al. Moisture absorption characteristics and mechanical degradation of composite lattice truss core sandwich panel in a hygrothermal environment. Composites Part A: Applied Science and Manufacturing, 2019; 127: 105647. doi: 10.1016/j.compositesa.2019.105647

[19] Feng Y, Ma B, Cui R, et al. Effects of hygrothermal environment on the buckling and postbuckling performances of stiffened composite panels under axial compression. Composite Structures, 2020; 242: 112132. doi: 10.1016/j.compstruct.2020.112132

[20] Zhang T, Li S, Chang F, et al. An experimental and numerical analysis for stiffened composite panel subjected to shear loading in hygrothermal environment. Composite Structures, 2016; 138: 107-115. doi: 10.1016/j.compstruct.2015.11.056

[21] Feng Y, He Y, An T, et al. Effect of hygrothermal condition on buckling and post-buckling performance of CCF300/5228A aero composite stiffened panel under axial compression. Journal of Reinforced Plastics and Composites, 2015; 34(12): 989-999. doi: 10.1177/0731684415585381

[22] ASTM: Standard test method for moisture absorption properties and equilibrium conditioning of polymer matrix composite materials. ASTM D5229/D5229M. West Conshohocken, PA: ASTM International.